Rare Metal Materials and Engineering
Volume 47, Issue 7, July 2018
Online English edition of the Chinese language journal

Available online at www.sciencedirect.com
ScienceDirect

Cite this article as: Rare Metal Materials and Engineering, 2018, 47(7): 2005-2010.

ARTICLE

Effect of Strain Rate on Microstructure and Mechanical Properties of TC18 Thick Plate by Electron Beam Welding

Han Wen[1,2], Fu Li[1], Chen Haiyan[1]

[1] State Key Laboratory of Solidification Processing, Northwestern Polytechnical University, Xi'an 710072, China; [2] The First Aircraft Institute, Xi'an 710089, China

Abstract: Influence of the strain rate on microstructures, tensile properties and strain hardening behavior of the electron beam welded joint of TC18 titanium alloy under optimized welding parameters was investigated with three slices (top, middle and bottom). The results show that the welding leads to significant microstructural changes across the joint. The microstructure of fusion zone is composed of coarsened β phase and secondary α-phase. Compared with the base metal, the joint slices along the thickness exhibits a lower strength and plasticity but a further higher hardening capacity. The strength and ductility of the bottom slices are higher than those of the middle and top slices. The maximum yield strength and ultimate tensile strength of the welding slices reach 83% of those of the base metal at the strain rate of 1×10^{-2} s^{-1} . The hardening capacity of welding slices decreases with increasing of the strain rate. Tensile fracture occurs in the weld zone. The fracture process of the top slice is cleavage fracture. However, the middle and bottom slices are quasi-cleavage crack.

Key words: electron beam welding; tensile properties; strain hardening behavior; strain rate

TC18 is a kind of high strength near β titanium alloy developed by Aviation Materials Institute of Soviet Union in 1970 s. It is mainly used in the manufacture of heavy forgings and various aircraft structures of high load-carrying capacity. Electron beam welding (EBW) is characterized by high heat concentration, large weld depth-width ratio, fast welding speed, good physical properties, small welding residual stress and deformation, and easy to realize high precision welding, which is one of the most common welding processes for titanium alloys [1-5]. Common defects in electron beam welding of thick plates are pores. Pores easily lead to stress concentration, so that the plastic joints reduce the fatigue life, and even lead to fracture rupture thick plate. O. Jinkeun et al[6] studied the microstructure and fatigue properties of titanium alloy electron beam welded and TIG welded joints. It was found that there were pores in the electron beam welded joints, and stress concentration in the pores made them a fatigue crack initiation source, leading to reduced high cycle fatigue strength of the joint. H. Q. Wu et al[7] studied the fracture mechanism of electron beam welded joints and found that the small pores distributed unevenly in the weld act as the source of crack initiation. There are few studies on the EBW joints of TC18 thick plate, especially inhomogeneity research of microstructure and mechanical properties for thick plates EBW joints. Investigation on microstructure and mechanical properties of TC18 EBW joints is of scientific significance and practical value in manufacture. Therefore, this study aimed at evaluating the strain rate effects on the mechanical properties of EBW for TC18 titanium alloy.

1 Experiment

The materials used in the present study are forged TC18 titanium alloys of 15 mm in thickness, with the chemical compositions listed in Table 1. All alloys were machined into the plates of 100 mm×75 mm×15 mm, and then mechanically and chemically cleaned before welding. EBW

Table 1 Chemical composition of TC18 (wt%)

Al	Mo	V	Cr	Fe	Ti
4.4~5.7	4.0~5.5	4.0~5.5	0.5~1.5	0.5~1.5	Bal.

Received date: July 15, 2017
Foundation item: Key Areas of Innovation Team in Shaanxi Province (2014KCT-12)
Corresponding author: Fu Li, Ph. D., Professor, State Key Laboratory of Solidification Processing, Northwestern Polytechnical University, Xi'an 710072, P. R. China, Tel: 0086-29-88460250, E-mail: fuli@nwpu.edu.cn

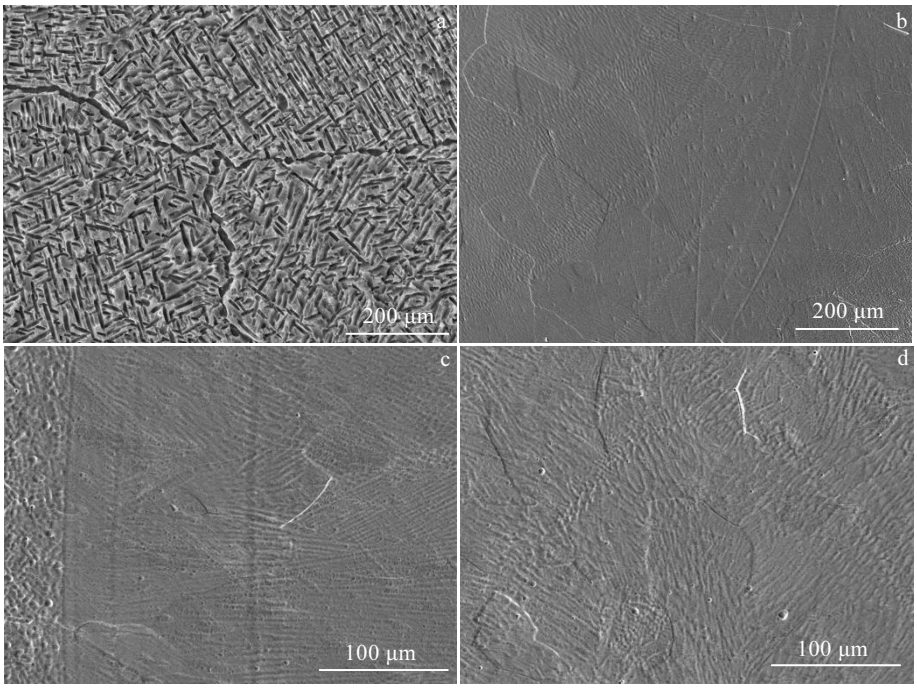

Fig.1 Microstructures of the BM and joint: (a) BM, (b) top, (c) middle, and (d) bottom

was performed using KS150-G150 machine with an accelerating voltage (V) of 60 kV, an electron current (I_b) of 23 mA, a focus current (I_f) of 2090 mA, and a welding speed (v) of 8 mm/s.

The cross-section of the welded joint was cut and ground with water abrasive papers, and then polished using diamond paste up to 1 μm. After etching with Keller's reagent (2 mL hydrofluoric acid, 8 mL nitric acid and 90 mL distilled water), the microstructure was examined by an optical microscope in conjunction with an image analysis system and an X-max20/INCA 250 scanning electron microscope (SEM) with three dimensional fractographic imaging capacities. Sub-sized tensile specimens, with a gauge length of 25 mm (i.e., a parallel length of 32 mm) and width of 6 mm in accordance with ASTM-E8 M standards, were cut perpendicularly to the welding directions and sliced equally into three pieces (top, middle and bottom) in the thickness direction, and then machined to the required dimensions using the electro-discharge wire cutting. The gauge area of specimens was ground with SiC papers up to a grit number of 600 along the loading axis to get rid of the cutting marks and to achieve a smooth surface. Tensile tests were conducted by a fully computerized tensile testing machine at a constant strain rate of 1×10^{-2}, 1×10^{-3}, 1×10^{-4} and 1×10^{-5} s^{-1} and room temperature. At least three samples were tested at each strain rate. The fracture surfaces of the base metal (BM) and EBW joints were examined by SEM.

2 Results and Discussion

2.1 Microstructure

The microstructures of the TC18 titanium alloy BM and EBW joint along the plate thickness by SEM are shown in Fig.1. It is seen that the BM consists of α+β phases. TC18 alloy is rich in β phase and is composed of basket-weave microstructure, and α phase precipitates uniformly within grains[8]. After EBW, a remarkable change in the microstructure occurs in fusion zone (FZ) as shown in Fig.1b~1d which illustrate typical microscopic structures of EBW TC18 titanium alloy through thickness from the top to the bottom. The microstructure of FZ is composed of coarsened β phase and secondary α phase. The weld is coarse columnar β crystal, and the grain near the seam is also seriously roughened. The base material is fine in α+β grain basket weaving, grain boundary α coarse and intermittent varying degrees. The microstructure of the weld is metastable β, because the thermal cycle of electron beam welding is very fast, and there is no crystal precipitation in the welding state. Part of solid solution of the heat-affected zone (HAZ) occurs at high welding temperature, and the original chip profile becomes coarse. The coarse metastable β grain leads to a severe decrease in impact toughness, strength and plasticity of the weld compared with the base metal. TEM observations show that the content of primary α phase decreases and the content of β phase increases from the BM to the weld in Fig.2. As the volume fraction of primary α phase decreases, the number of un-transformed β structure and the secondary α phase

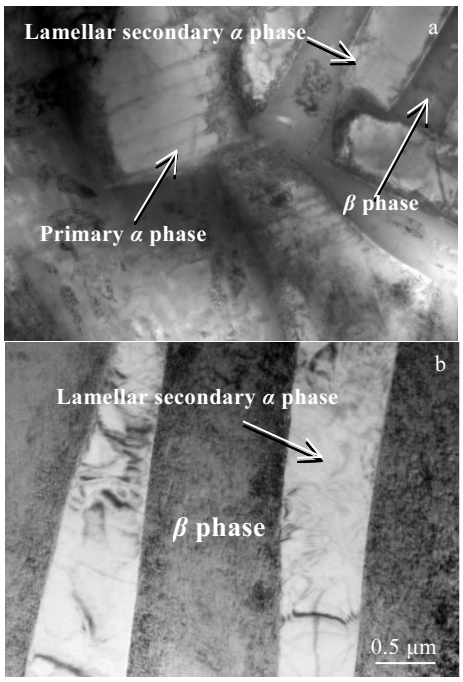

Fig.2 TEM images of BM (a) and FZ (b) (bottom slice of samples)

diffusely distributed on it increase. The number of secondary α phases distributed increase, and the interface between the two phases increases, resulting in the enhancement of the strengthening effect of the second phase and the increase of the strength of FZ. The grain size of columnar β decreases gradually, causing a tortuous path when the crack passes it quickly, and the deformation of the alloy increases, so the elongation increases and the plasticity increases. The same pattern appears from the top to the bottom of the weld.

2.2 Tensile properties

Fig.3 shows the tensile stress-strain curves of the TC18 BM and different (top, middle, and bottom) slices of EBW samples tested at different strain rates. It is seen that the strength and ductility of the welded joint are less than that of the base material. The bottom slices exhibit the higher strength and ductility than the middle and top slices. This is directly associated with the microstructure and grain morphology (Fig.1). Fig.4 shows the effect of strain rate on yield strength, Ultimate tensile strength and ductility of BM, top, middle and bottom slices of samples. It has the same result with Fig.3. The strength and the ductility basically increase for different (top, middle, and bottom) slices with increasing strain rate.

The mechanical property is closely related to the structure. Compared with the BM, the structure of EBW slices has significant changes. The FZ changes from basket-weave microstructure and dispersed grain α to columnar crystals which is shown in Fig.1. The strength and plasticity decrease obviously. Non-uniform distribution structure along the plate thickness for joint determine that the strength and plasticity are different along the plate thickness. The top of the joint is wide and has coarse grains,

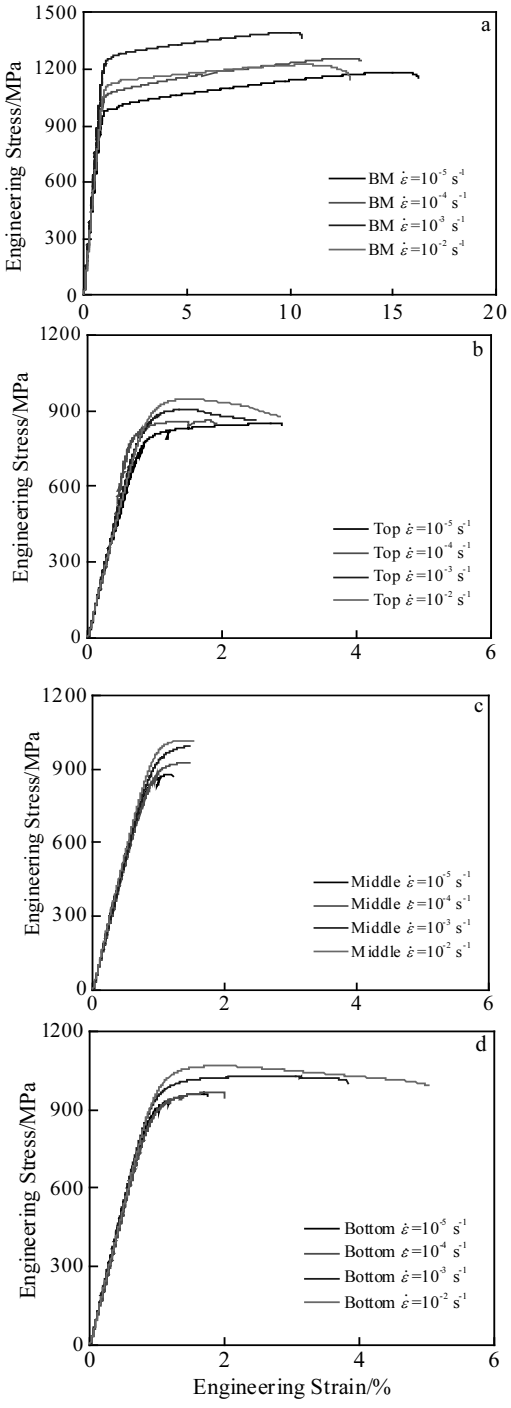

Fig.3 Tensile stress-strain curves of TC18 BM (a) and the different slices of samples by electron beam welding at different strain rates: (b) top, (c) middle, and (d) bottom

which lead to the lowest intensity. Compared with the top slices, the middle and bottom slices are narrow, and the grain size of the middle slices are bigger than that the bottom. So the intensity of the bottom slices is higher than of the middle and the top.

The plastic deformation mechanism changes the Ti-6Al-4V alloy intensity by strain rate. The major deformation mechanisms are found to be dislocation glide at low strain rate. But it changes into twin at high strain rate[9]. The TC18 alloy is a type of α-β titanium alloy which is rich in β-stablizing elements. The increase of strain rate results in the increase of dislocation density. It changes into twin at high strain rate, and then the intensity increase too.

2.3 Strain hardening behavior

The hardening capacity (H_c) of a material was defined as[10]:

$$H_c = \frac{\sigma_{UTS} - \sigma_{YS}}{\sigma_{YS}} = \frac{\sigma_{UTS}}{\sigma_{YS}} - 1 \quad (1)$$

Where σ_{UTS} is the UTS and σ_{YS} is the YS of the material. The obtained hardening capacity of the BM and the EBW slices through thickness are shown in Fig.5. The hardening capacity of EBW slices decreases with increasing strain rate. The hardening capacity is significantly enhanced at the middle and bottom slices compared with the top slice. Normally, when a material is strengthened, the YS increases while the hardening capacity decreases since the capacity of dislocation storage decreases during plastic deformation[11, 12].

Fig.6 shows a Kocks-Mecking type plot of strain hardening rate (d_σ/d_ε) vs. net flow stress (σ-σ_y) at a strain rate of 1×10^{-2} s^{-1}. It is seen that the strain hardening rate decreases linearly in the BM and EBW samples, exhibiting stage III strain hardening behavior followed by stage IV hardening, due to the occurrence of dynamic recovery as the stress reaches a point where dislocation annihilations takes place in stage III [13], without the presence of stage I hardening (or 'easy glide' which depended strongly on the orientation of the crystal) or stage II linear hardening with a constant strain hardening rate. The EBW samples exhibit stage III strain hardening behavior while the BM has stage III and IV. Maybe it is because of the stacking fault energy. The stacking fault energy for titanium alloy is 0.35 J/m^2 [14]. In the materials with higher stacking fault energy, the occurrence of stage III will limit the range of stage II or make the stage II become an independent stage [11]. The strain hardening rate of the base metal and the section decreases linearly during Stage III, and the strain hardening rate of the base material slightly decreases during Stage IV. The plasticity of the base metal is good, because the stress reaches the stage III of the strain hardening after dislocation quench dynamic response, the base material shows strain hardening IV stage immediately after III stage.

Consistent with the hardening capacity, the strain hardening rate of the middle and bottom EBW joint slices are higher than that of the BM and top slice in both stages III and IV. Strain hardening of a material is sensitive to the dislocation strain field interaction, hence the Taylor dislocation contribution ($\sigma_d=M_\alpha Gb\rho^{1/2}$) is significant[13], where G is the shear modulus, b is the Burgers vector, M is the Taylor factor and α is a constant. As the number of dislocations increases during deformation, the spacing among them becomes smaller and their interactions are more repulsive, which ultimately increase the resistance to deformation. On the other hand, the higher strain hardening rate in the EBW joints at higher strains or later stage of deformation might can be attributed to the larger grain size in the FZ, since the larger grain size leads to the stronger dislocation storage capacity at later stage of higher strains.

2.4 Fractography

Fig.7 shows the fracture surfaces of the TC18 BM and different slices of EBW samples tested at a strain rate of 1×10^{-4} s^{-1}. The fracture morphology in the BM is characterized by the ductile fractures with a plenty of equiaxed and tearing dimples (Fig.7a). The fracture morphology of the top section shows quasi-cleavage and intergranular dimple fracture features with lots of cleavage steps, river patterns and tearing ridges. From middle to

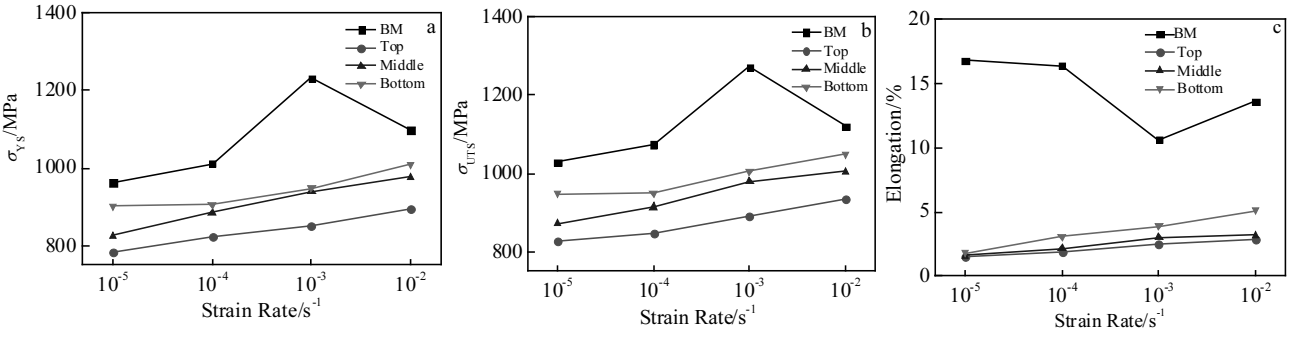

Fig.4 Effect of strain rate on yield strength (σ_{YS}) (a), ultimate tensile strength (σ_{UTS}) (b), and elongation (c) of BM, top, middle and bottom slices of samples by electron beam welding

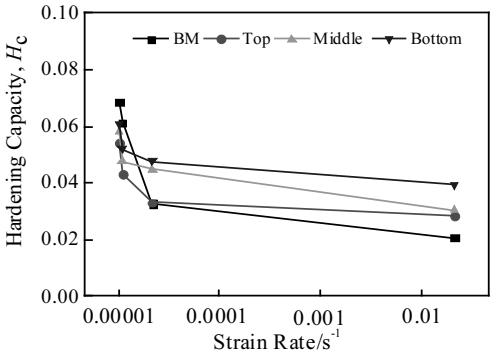

Fig.5 Effect of strain rate on the hardening capacity of BM, top, middle and bottom slices of joints by electron beam welding

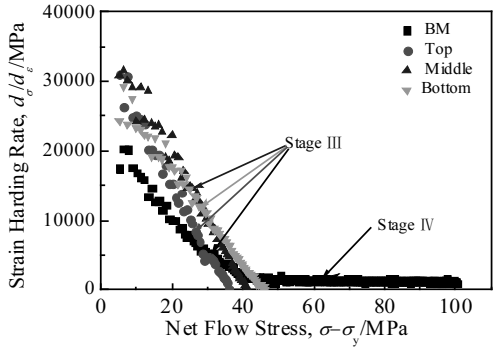

Fig.6 Strain hardening rate vs net flow stress (σ-σ_y) in BM and joint slices by electron beam welding (top, middle and bottom) along the thickness direction tested at a strain rate of 1×10^{-2} s^{-1}

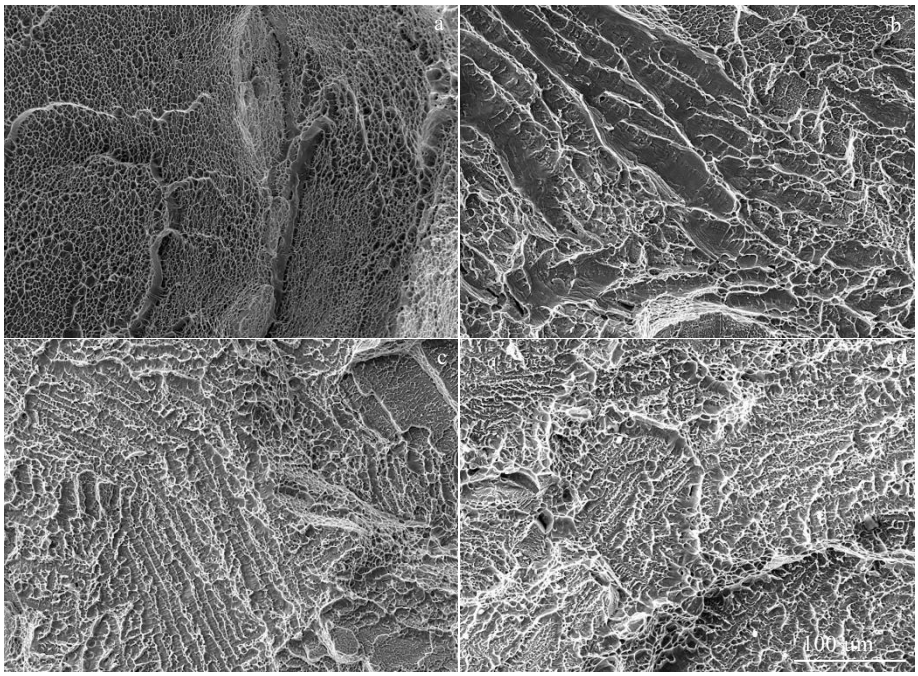

Fig.7 Tensile fracture morphologies of the TC18 BM (a), top (b), middle (c), and bottom (d) of EBW samples at a strain rate of 1×10^{-4} s^{-1}

bottom the cleavage steps decrease and the dimples increase. The reason can be explained from the microstructure and grain morphology of the TC18 BM and different slices of EBW samples. More detailed analysis has been discussed in Sections 2.1 and 2.2. As discussed above, the BM shows better ductility than FZ, and the bottom shows better ductility than the top of the joint.

3 Conclusions

1) The microstructure across the welded joint exhibits a considerable change, mainly consisting of coarsened β phase and secondary α phase in the FZ. The grain size of columnar β in the bottom is finer than that in the top.

2) Compared with the BM, the joint slices along the thickness exhibits a lower strength and plasticity. The maximum YS and UTS of the weld slice is obtained to be 893 MPa and 933 MPa, respectively at the strain rate of 1×10^{-2} s^{-1}, which reach 83% of those of the base metal. The bottom slices exhibit the higher strength and ductility than the middle and top slices. The strength and the ductility basically increase for different slices with increase of the strain rate.

3) The hardening capacity is dying down at lower strain rates, but is significantly enhanced for EBW slices at higher strain rates. The hardening capacity is significantly

enhanced for the middle and bottom slices compared with for the top slice and decreases through thickness with increase of the strain rate for the base metal and the EBW slices.

4) The EBW samples exhibit stage III strain hardening behavior. Consistent with the hardening capacity and strain hardening exponent, the strain hardening rate of the middle and bottom EBW joint slices is higher than that of the top slice.

5) The welded joints fail in weld zone. The fracture process of the top slice is cleavage fracture, but the fracture process of the middle and bottom slices are quasi-cleavage crack.

References

1 Luo L, Mao X N, Yang G J *et al*. *Material & Heat Treatment*[J], 2009, 38(14): 14

2 Huda Z, Edi P. *Materials and Design*[J], 2013, 46: 552

3 Zhu X J, Tan M J, Zhou W. *Scripta Materialia*[J], 2005, 52: 651

4 Holmquist M, Recina V, Pettersson B. *Acta Materialia*[J], 1999, 47(6): 1791

5 Li S J, Murr L E, Cheng X Y *et al. Acta Materialia*[J], 2012, 60: 793

6 Jinkeun O, Nack J K, Sunghak L *et al*. *Materials Science and Engineering A*[J], 2003, 340: 232

7 Wu H Q, Feng J C, He J S *et al*. *Transactions of the China Welding Institution*[J], 2004, 25(4): 59

8 Li A B, Huang L J, Meng Q Y *et al*. *Materials and Design*[J], 2009, 30: 1625

9 Zhou W, Chew K G. *Journal of Materials Science*[J], 2002, 37: 5159

10 Afrin N, Chen D L, Cao X *et al*. *Scripta Materialia*[J], 2007, 57(11): 1004

11 Tane M, Nakano T, Kuramoto S. *Acta Materialia*[J], 2011, 59: 6975

12 Chen X H, Pan F S, Mao J J *et al. Materials and Design*[J], 2011, 32: 1526

13 Kocks U F, Mecking H. *Progress in Materials Science*[J], 2003, 48: 171

14 Morán-López J L, Mejía-Lira F, Sanchez J M *et al*. *Structural and Phase Stability of Alloys*[M]. New York: Plenum Press, 1992: 65

应变速率对 TC18 钛合金厚板电子束焊接接头组织和力学性能的影响

韩　文[1,2]，傅　莉[1]，陈海燕[1]

(1. 西北工业大学 凝固技术国家重点实验室，陕西 西安 710072)

(2. 航空工业第一飞机设计研究院，陕西 西安 710089)

摘　要：研究了在优化后的焊接工艺参数下，TC18 钛合金厚板电子束焊接接头沿板厚方向（上层、中层、下层）应变速率对显微组织、拉伸性能和应变硬化行为的影响。结果表明：焊接后焊缝微观结构发生了明显变化，熔合区显微组织由粗大的 β 相和次生 α 相组成。与母材相比，沿厚度方向的焊接接头表现出较低的强度和塑性，但其硬化能力增强。焊缝下层的强度和延伸率高于中层和上层。当应变速率为 1×10^{-2} s^{-1} 时，焊缝的最大屈服强度和极限抗拉强度达到母材的 83%。随着应变速率的增加，焊缝的硬化能力下降。拉伸断裂发生在焊缝区，上层的断裂过程为解理断裂，中下层为准解理断裂。

关键词：电子束焊接；拉伸性能；应变硬化行为；应变率

作者简介：韩 文，女，1982年生，硕士，西北工业大学材料学院，陕西 西安 710072, E-mail: 13109515354@126.com